ARTICLE

Hierarchically Structured Titania Films Prepared by Polymer/Colloidal Templating

Gunar Kaune,[†] Mine Memesa,[‡] Robert Meier,[†] Matthias A. Ruderer,[†] Alexander Diethert,[†] Stephan V. Roth,[§] Maria D'Acunzi,[‡] Jochen S. Gutmann,[||] and Peter Müller-Buschbaum*[,†]

Physik-Department E13, Technische Universität München, James-Franck-Strasse 1, 85747 Garching, Germany, Max-Planck-Institut für Polymerforschung, Ackermannweg 10, 55128 Mainz, Germany, HASYLAB at DESY, Notkestrasse 85, 22603 Hamburg, Germany, Max-Planck-Institut für Polymerforschung, Ackermannweg 10, 55128 Mainz, Germany, and Institut für Physikalische Chemie, Johannes Gutenberg-Universität, Welderweg 11, 55099 Mainz, Germany

ABSTRACT Hierarchically structured titania films for application in hybrid solar cells are prepared by combining microsphere templating and sol−gel chemistry with an amphiphilic diblock copolymer as a structure-directing agent. The films have a functional structure on three size scales: (1) on the micrometer scale a holelike structure for reduction of light reflection, (2) on an intermediate scale macropores for surface roughening and improved infiltration of a hole transport material, and (3) on a nanometer scale a mesoporous structure for charge generation. Poly(dimethyl siloxane)-*block*-methyl methacrylate poly(ethylene oxide) (PDMS-*b*-MA(PEO)) is used as a structure-directing agent for the preparation of the mesopore structure, and poly(methyl methacrylate) (PMMA) microspheres act as a template for the micrometer-scale structure. The structure on all levels is modified by the method of polymer extraction as well as by the addition of PMMA particles to the sol−gel solution. Calcination results in structures with increased size and a higher degree of order than extraction with acetic acid. With addition of PMMA a microstructure is created and the size of the mesopores is reduced. Already moderate microstructuring results in a strong decrease in film reflectivity; a minimum reflectivity value of less than 0.1 is obtained by acetic acid treatment and subsequent calcination.

KEYWORDS: hierarchical structures • titanium dioxide • porous materials • polymer templating • GISAXS

INTRODUCTION

Structuring of titania thin films on a nanometer scale has attracted considerable attention in the past few years, since nanostructured titania shows outstanding properties and has widespread application potentials: e.g. in photovoltaics, photocatalysis, and gas sensing (1−6). Due to its semiconducting properties, titania enhanced the fast growth of organic photovoltaics in terms of the dye-sensitized solar cell (7−9), which combines a mesoporous titania network and a hole-conducting electrolyte or organic material to generate electric power from sunlight. A crucial point on the way to efficient devices is a precise control of the film morphology, since the morphology determines the active surface area and therefore has a direct influence on the efficiency of the device. Numerous preparation methods have been applied for preparation of nanostructured titania films (10−14), resulting in a variety of morphologies such as nanoparticles, nanowires, vesicles, lamellae, and mesoporous structures (15−18). As a very promising route the application of sol−gel chemistry in combination with block copolymer templates has been developed (19−22). In this approach a phase separation is induced in an amphiphilic block copolymer by a so-called good−poor solvent pair (23, 24), while a titania precursor is chemically linked to one of the blocks. By thin film preparation techniques such as spin coating or solution casting, the structure in the sol−gel solution is transferred to solid films with titania particle arrays embedded in a polymer matrix. After removal of the matrix, e.g. by UV degradation or solvent extraction, a scaffold of amorphous titania particles ordered on the nanometer scale remains, which can be transformed to crystalline titania by subsequent heat treatment.

One limitation of block copolymer templating is the preference of structures with only one characteristic length on the order of several nanometers, whereas in many applications hierarchically structured materials with a superstructure on a larger size scale are favorable (25−27). In the case of hybrid or dye-sensitized solar cells a mesoporous network is required for efficient charge generation, while a secondary structure on a micrometer scale enhances light scattering, resulting in improved absorption characteristics and thus a more efficient device (28). A number of techniques have been applied for preparation of hierarchically structured films; usually sol−gel chemistry with a surfactant as template is combined with a second technique to create a structure on a larger length scale. Yang et al. used a combination of triblock copolymer templating, colloidal particles, and micromolding to prepare films with three structural levels (29). In alternative approaches a controlled

* To whom correspondence should be addressed. E-mail: muellerb@ph.tum.de.

Received for review September 1, 2009 and accepted October 29, 2009

[†] Technische Universität München.

[‡] Max-Planck-Institut für Polymerforschung.

[§] HASYLAB at DESY.

[||] Max-Planck-Institut für Polymerforschung and Institut für Physikalische Chemie.

DOI: 10.1021/am900592u

Published on Web 11/12/2009

Scheme 1. Illustration of the Applied Preparation Route for Hierarchical Structuring of Titania

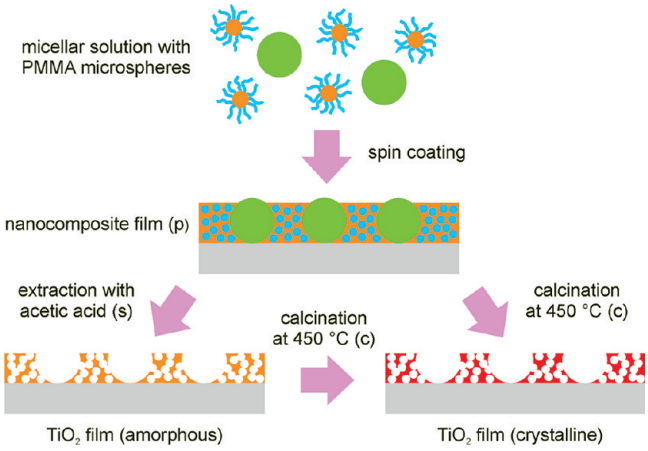

phase separation was induced by addition of a polymer (30, 31) or an electrohydrodynamic deposition technique was used (32) to create a superstructure. With the latter technique Zhao et al. prepared hierarchically structured titania films and applied them in a in a dye-sensitized solar cell, which showed an increased power conversion efficiency (32).

Recently we reported about the use of poly(ethylene oxide) methyl methacrylate-*block*-poly(dimethyl siloxane)-*block*-methyl methacrylate poly(ethylene oxide) ((PEO)MA-*b*-PDMS-*b*-MA(PEO)) triblock copolymer for the preparation of nanostructured titania thin films (33). In this work we used the corresponding diblock copolymer, poly(dimethyl siloxane)-*block*-methyl methacrylate poly(ethylene oxide) (PDMS-*b*-MA(PEO)), for the preparation of films with functional hierarchical structures. A mesoporous structure for charge separation is introduced by the diblock copolymer template, and an additional structure on a micrometer scale for reduction of light reflection is established by colloidal particles as a secondary template. We used microspheres of poly(methyl methacrylate) (PMMA) grafted with PDMS having a diameter of 1 μm (35), which were added to the sol–gel precursor solution and removed after spin coating of the films. The resulting depressions with well-defined size and shape in the titania film (see Scheme 1) act as light scatterers to allow a higher portion of incoming light to be trapped. The removal of the polymer templates was done in two ways. Acetic acid was used to remove the PDMS-*b*-MA(PEO) and PMMA templates by solvent extraction, and additionally some films were annealed at 450 °C. Alternatively, the as-prepared films were calcined at the same temperature to burn away the templating polymers. The installed structures were analyzed by scanning electron microscopy (SEM) and grazing incidence small-angle X-ray scattering (GISAXS). UV/vis spectroscopy was used to quantify the effect of the microstructure on the film reflectivity.

EXPERIMENTAL SECTION

Polymer Synthesis. The PDMS-*b*-MA(PEO) diblock copolymer was synthesized by atomic radical polymerization of (PEO)MA monomer via PDMS-Br macroinitiator. For the synthesis of the macroinitiator, hydroxyl terminated PDMS (ABCR Gelest, Karlsruhe, Germany) (5000 g/mol; 10 g, 2 mmol) was dissolved in anhydrous THF (distilled from a THF, butyllithium, and 1,1-diphenylethylene mixture) (300 mL). Anhydrous triethylamine (1.4 mL, 10 mmol) was added to the stirred solution, followed by addition of 2-bromo-2-methylpropionyl bromide (99% Aldrich, Steinheim, Germany) (0.62 mL, 5 mmol). The mixture was stirred overnight at ambient temperature. It was filtered to remove the bromide salt, and the solvent was evaporated under vacuum. The resulting colorless oil was diluted with dichloromethane (Aldrich) (400 mL), put into an extraction funnel, and washed with saturated sodium bicarbonate solution. The organic layer was isolated and dried over anhydrous magnesium sulfate, with a yield of 82% by weight. ^{1}H NMR spectra were recorded on a Bruker DRX-300 NMR instrument using $CDCl_3$ as the solvent. ^{1}H NMR of PDMS-Br (300 MHz): δ 0.05 (m, 6H), 0.53 (m, 4H), 1.61 (m, 4H), 1.94 (s, 3H), 2.00 (s, 3H), 3.44 (t, 4H), 3.68 (t, 4H), 4.32 (t, 4H).

The macroinitiator (3 g, 0.6 mmol) was put into a reaction flask and dissolved in dry THF (20 mL) under argon flux. The (PEO)MA monomers (3 g, 6.3 mmol), Cu$^{\text{I}}$Br (0.205 g, 1.44 mmol), and *N*,*N*,*N*′,*N*′,*N*″-pentamethyldiethylenetriamine (PMDETA, 99% Aldrich) (125 μL, 0.6 mmol) were added after purging with argon. Three freeze–pump–thaw cycles were applied to remove any residual oxygen from the reaction medium. The polymerization was concluded at 32 °C under argon for 6 days and stopped by exposure to air. After addition of a Dowex ion exchanger, the mixture was filtered by passing through aluminum oxide (Al_2O_3) and centrifuged at 4000 rpm for 15 min. The clear solution above the Al_2O_3 was taken up, and the remaining solvent was evaporated off, yielding 94% by weight of the diblock copolymer as a clear viscous liquid. ^{1}H NMR of PDMS-*b*-MA(PEO) (300 MHz): δ 0.05 (m, 6H), 0.5–2.2 (acrylate backbone peaks with peaks from **2**), 3.37 (s, 3H), 3.64 (t, 4H).

The number-average molecular weight of PDMS-*b*-MA(PEO) is 5000 g/mol for PDMS and for MA(PEO) is 3000 g/mol; the polydispersity is 1.68.

PMMA microspheres grafted with PDMS were synthesized according to the literature (35). The microspheres are dispersed in hexane and have a mean diameter of 1.00 ± 0.01 μm.

Sample Preparation. Silicon wafers were used as substrates and cleaned before use in a basic bath (36).

For the film preparation PDMS-*b*-MA(PEO) (0.269 g) was dissolved in a mixture of THF (3.02 g) and isopropyl alcohol (1.00 g); afterward HCl (37%, 0.045 g) as selective solvent and titanium tetraisopropoxide (TTIP, 0.134 g) were added dropwise. After the mixture was stirred for about 1 h, PMMA microspheres in amounts of 0.86, 2.9, and 8.6 mg, corresponding to 3%, 10%, and 30% PMMA weight fraction with respect to PDMS-*b*-MA(PEO), were added to 0.5 mL of the sol–gel solution and the solution was spin coated immediately to avoid dissolution of the PMMA. Spin coating was done on a Süss MicroTec Delta6 RC spin coater under ambient conditions (temperature 24 °C, relative humidity 31%) with 2000 rpm for 60 s. To extract the PDMS-*b*-MA(PEO) and PMMA from the nanocomposite films, the films were immersed in acetic acid for 2 min after storage for at least 12 h and subsequently rinsed with deionized water. Alternatively, calcination was carried out for 4 h at 450 °C in air with a heating rate of 6.25 °C/min, starting from room temperature. The acetic acid treated and calcined films were heated under the same conditions. Scheme 1 shows an overview of the individual steps in the film preparation.

Film Characterization. SEM images were taken with a field emission SEM (Zeiss LEO 1530 Gemini) operated at an accelerating voltage of 3 kV and at low working distances (WD) from 1 to 3 mm.

GISAXS experiments were performed at the beamline BW4 at HASYLAB (Hamburg, Germany) in ultrasmall angle geometry at a wavelength of 0.138 nm and a sample−detector distance of 13.96 m. A setup of high-quality entrance slits and a mostly evacuated pathway was used. Moderate microbeam focusing was achieved by the use of beryllium compound refractive lenses (beam size 40 μm × 40 μm) (37). The samples were placed horizontally in the sample chamber. The incidence angle was fixed to 0.413° and the scattering signal was recorded with a two-dimensional (2D) detector (MAR CCD camera, 79 μm pixel size). In front of the detector two separate beam stops were installed at the position of the direct beam and the specular peak to shield the detector.

Reflectivity spectra were measured with a PerkinElmer Lambda35 UV/vis spectrometer in reflection geometry in a wavelength range from 190 to 1100 nm. A scan rate of 120 nm/min and a slit width of 1 nm were used.

Film thickness was determined with a Filmetrics F20 thin film measurement system. The illuminated sample area was several square millimeters, and a wavelength range from 340 to 1100 nm was used to analyze the characteristic interference oscillations in the reflectance spectrum.

RESULTS AND DISCUSSION

Hierarchically structured titania films were prepared as described in the Experimental Section and analyzed with SEM and GISAXS. Figure 1 shows the SEM images of an PDMS-*b*-MA(PEO)-titania nanocomposite film prepared with PMMA microsphere addition in a concentration of 10% (with respect to the PDMS-*b*-MA(PEO) weight fraction in the sol−gel solution), together with images of the titania films obtained after removal of the templating polymers. For polymer removal solvent extraction, solvent extraction followed by calcination, or direct calcination of the spin coated films were applied. The high-magnification image of the as-prepared nanocomposite film shows a structure of titania particles embedded in a polymer matrix; additionally the surface is structured by embedded pores of about 200 nm in diameter. These macropores are a result of a liquid/liquid phase separation during spin coating (38). The PMMA microspheres appear as bright spots in the films, and it can be seen that the particles tend to aggregate in the solution and are inhomogeneously distributed in the film. When the nanocomposite film is treated with acetic acid, the PMMA microparticles as well as the PDMS-*b*-MA(PEO) matrix are removed and the titania structure becomes visible. Because of the methacrylate chain in the MA(PEO) block the PDMS-*b*-MA(PEO) matrix is soluble in acetic acid and can be removed together with PMMA in an acetic acid bath, which allows the removal of both polymer templates in one step instead of applying different solvents in consecutive extraction steps. The obtained titania film has a mesoporous, spongelike structure with partially interconnected pores of circular shape and a diameter of about 30−40 nm. The size is far above 10 nm, a limit which has often been observed in films prepared with surfactant or block copolymer templated films (39). This large pore size opens new possibilities for the use of hole conducting materials with characteristic dimensions larger than 10 nm, i.e. semiconducting polymers with a high molecular weight, which can easily be infiltrated in the porous network. At the same time the pores are small

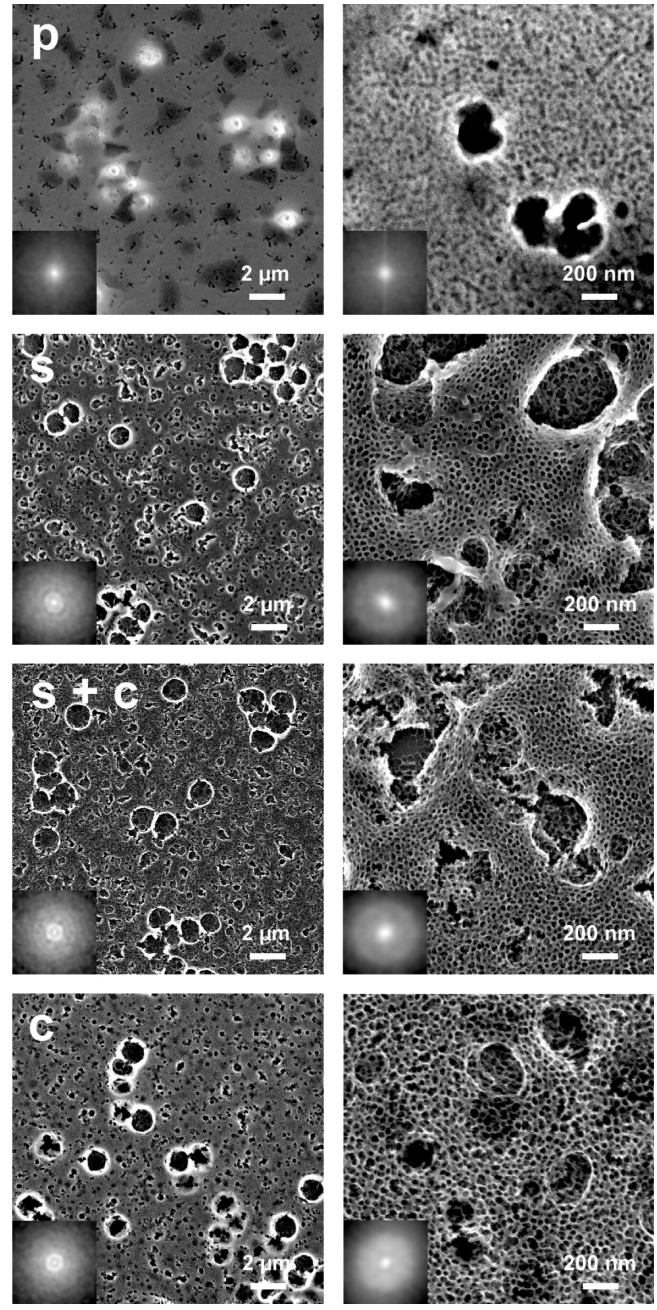

FIGURE 1. SEM images of an as-prepared nanocomposite film (p), an acetic acid treated film (s), an acetic acid treated and calcined film (s + c), and a directly calcined film (c). In the images with low magnification (left) the macropores and the surface depressions are visible, whereas the images with high magnification (right) give detailed views of the macro- and mesopore structures.

enough to be on the scale of the diffusion length of excitons and to provide the high surface area being necessary for exciton separation, making the films suited for preparation of solar cells with sufficient photovoltaic response.

As secondary structure in the images, macropores resulting from the spin coating process are visible, with an irregular shape and eroded edges from the acetic acid treatment. Their size is above 100 nm; thus, they are well distinguished from the mesopore structure. Due to these macropores the surface is additionally roughened and they provide channels to the pore structure for the infiltration of

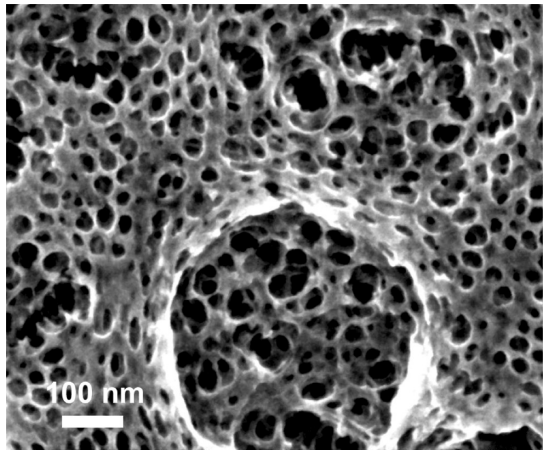

FIGURE 2. Detailed view of structural levels in the acetic acid treated film. The macropores are further structured by the mesopores, which extend into the bulk of the film.

the hole conducting material. It is known that such a superstructure of the mesopore structure can increase the efficiency of a dye-sensitized solar cell significantly (32). The large-scale images additionally show craterlike surface depressions of about 1 μm in diameter, which originate from the dissolved PMMA microspheres and form a third structural level in the film. These depressions act as additional scatterers for incoming light; thus, reflection is reduced and a higher portion of light can be converted into excitons. A detail of the structure is shown in Figure 2. It is clearly visible that the mesopore structure is not only present at the surface but also extends into the bulk of the sample and is also found at the bottom of the macropores.

Calcination of the acetic acid treated film does not change the film morphology significantly. Primarily remaining traces of the polymer templates are removed, and the crystalline structure of the titania is modified. When the spin coated film is calcined without prior acetic acid treatment, the resulting titania morphology is comparable to the morphology obtained by solvent extraction. Differences are visible in the appearance of the macropores, which maintain a more circular shape, and the film surface, which is not as eroded as by the treatment with acetic acid. Furthermore, the pore size is slightly increased.

In the case of polymer extraction also the film thickness is determined. The acetic acid treated films are 190 nm thick, whereas a subsequent calcination does not further modify the film thickness. Direct calcination results in thicker films with a thickness of 250 nm. A possible reason for this difference is a different structural contraction during the removal of the polymer templates; in the treatment with acetic acid the titania structures are more densified than in the heat treatment.

To study the influence of the PMMA microsphere addition on the film morphology, films from sol–gel solutions with 0%, 3%, and 30% PMMA particle content with respect to the amount of PDMS-*b*-MA(PEO) were prepared and calcined to remove the templating polymers. SEM images were again taken to characterize the installed titania structure (Figure 3). With increasing PMMA microsphere addition, as expected, the number of surface depressions created in the films increases, together with the tendency for agglomeration. In the film prepared with 30% PMMA most of the depressions are grouped and only a few are isolated. Furthermore, from both the images with low and high magnification it is visible that the fraction of PMMA particles in the sol–gel solution also influences the appearance of the macropores in the surface. In the film prepared without PMMA addition the macropores have a well-pronounced circular shape and are isolated from each other. When PMMA particles are added, the macropores are arranged in groups and show a more eroded, irregular appearance. Because THF is a good solvent for PMMA, parts of the PMMA particles are etched and PMMA is added as a ternary component to the sol–gel solution, which modifies the phase diagram and results in different phase separation behavior; thus, the morphology of the films, in particular the appearance of the macropores, is modified as well.

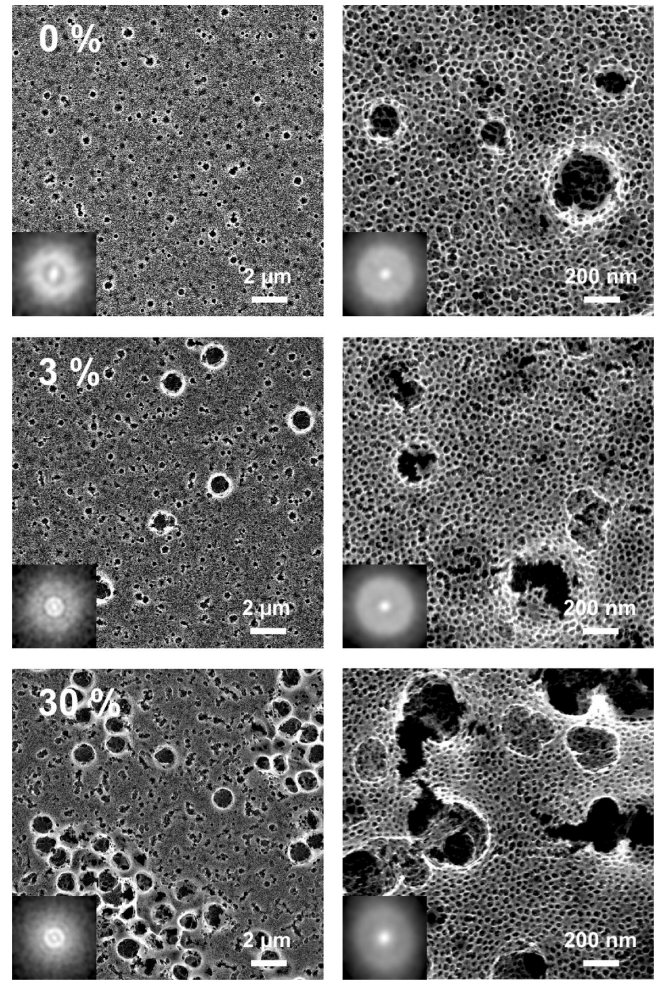

FIGURE 3. SEM images of titania films with 0%, 3%, and 30% amounts of PMMA microspheres added to the sol–gel solution. With increasing PMMA addition also the macro- and the mesopore structure is modified.

The structure installed in the films was further investigated with GISAXS (40). In contrast to microscopy methods with GISAXS the whole volume of the sample is probed and structures buried beneath the surface are detected. The scattering signal is averaged over a macroscopic sample

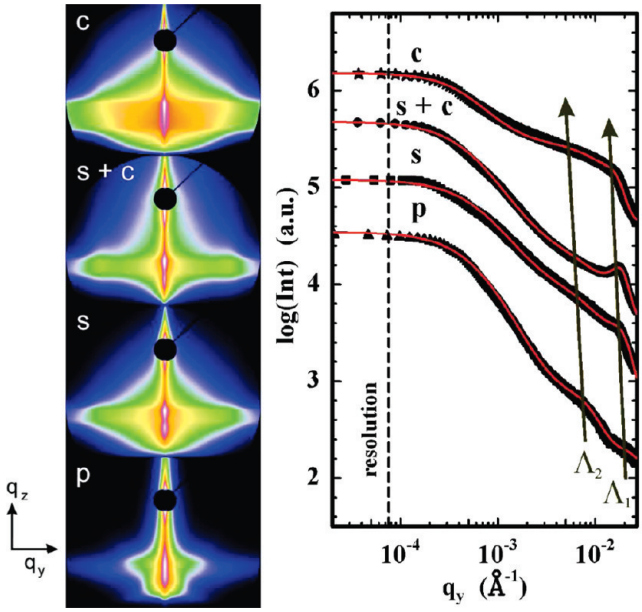

FIGURE 4. GISAXS scattering images (left) and corresponding cuts (right) of an as-prepared nanocomposite film (p), an acetic acid treated film (s), an acetic acid treated and calcined film (s + c), and a directly calcined film (c). Solid lines are fits to the data. Two preferred lateral lengths, Λ_1 and Λ_2, are present in the films.

area; thus, only structures being uniform over a large area are probed. The scattering patterns recorded from films with different template removal treatments together with the scattering pattern of the nanocomposite film are shown in Figure 4. Whereas the nanocomposite film (p) only shows weak diffuse scattering with the major intensity concentrated along the scattering plane, in the images of the titania films a broad diffuse scattering is visible, which is enhanced strongly in case of the calcined films (c, s + c). In particular, in the image of the acetic acid treated and calcined film (s + c) a well-pronounced side maximum is found, which corresponds to the preferred lateral length Λ_1 in the film structure and shows the high degree of order present in the titania nanostructure.

To analyze the 2D scattering patterns quantitatively, cuts along the q_y direction were taken from the images at an angle of 0.19° ($q_z = 0.048$ Å^{-2}), the position of the side maximum. From the cuts, information about the lateral structures in the films is provided (40). All cuts show a peak maximum, whose position shifts depending on the sample treatment. In comparison to the nanocomposite film (p), for the titania films the maximum is shifted to higher q_y values, corresponding to a smaller preferred structural length in the sample. The width of the maximum changes, depending on the sample treatment. The sharpest maximum is obtained for the acetic acid treated and calcined film (s + c), in accordance with the pronounced side maximum in the 2D image. For quantitative analysis the cuts were fitted in the effective surface approximation of the distorted wave Born approximation (DWBA) (40) by assuming polydisperse objects with a well-defined lateral dimension Λ_1 and a secondary structure with the characteristic length Λ_2, whereas Λ_1 and Λ_2 are the mean values of a Lorentzian distribution with widths σ_1 and σ_2, respectively (Figure 5). The structural

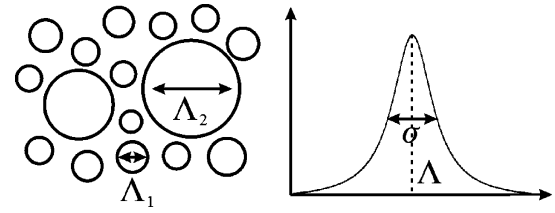

FIGURE 5. Schematic illustration of the parameters used for fitting the GISAXS cuts.

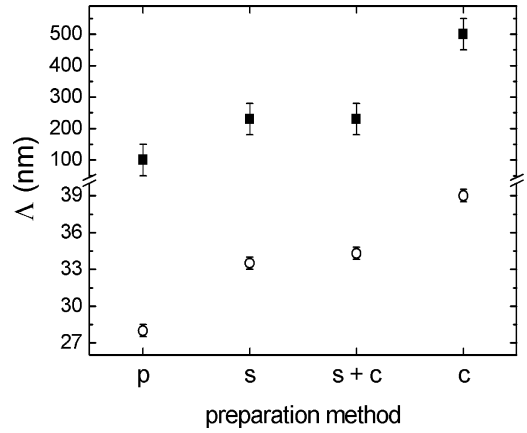

FIGURE 6. Preferred lateral lengths Λ_1 (open circles) and Λ_2 (solid squares) for different preparation methods extracted from the GISAXS cuts. With calcination the pore size and the size of the macropores are increased compared to those for the acetic acid treatment.

length Λ_1 is attributed to the block copolymer templated structure and represents the pore size, and the structural length Λ_2 results from the macropores and gives their mean dimension. Due to the broad size distribution of the macropores in the scattering images they appear as only a broad shoulder instead of a sharp peak. Taking the experimental resolution function into account, the parameters Λ_1, Λ_2, σ_1, and σ_2 were fitted. Figure 6 summarizes the preferred structural lengths extracted from these fits. The pore size increases when the polymer matrix is removed from the nanocomposite film, whereas calcination results in larger mesopores in comparison to those from solvent extraction (39 nm compared to 34 nm). Together with the higher film thickness this result suggests a higher porosity of the calcined films. Calcination after solvent extraction does not have a significant influence on the pore size; the mean value is 34 nm, as in the acetic acid treated film. A similar behavior is observed for the macropores; their size increases from 100 nm in the nanocomposite film to several hundred nanometers in the calcined film.

The analysis of the Yoneda peak positions in the scattering images allows an estimate of the film porosity. The Yoneda peak of a material is located at its critical angle of reflection; thus, from the peak position the material density can be calculated. In the case of mesoporous materials this density is an effective value averaged over the dense pore walls and the included pore volume. By assumption of unfilled pores ($\rho = 0$) the analysis of the Yoneda peak position of the acetic acid treated film reveals a mass density of 1060 g cm^{-3}, corresponding to a porosity of 72%. The acetic acid treated and annealed film has a mass density of

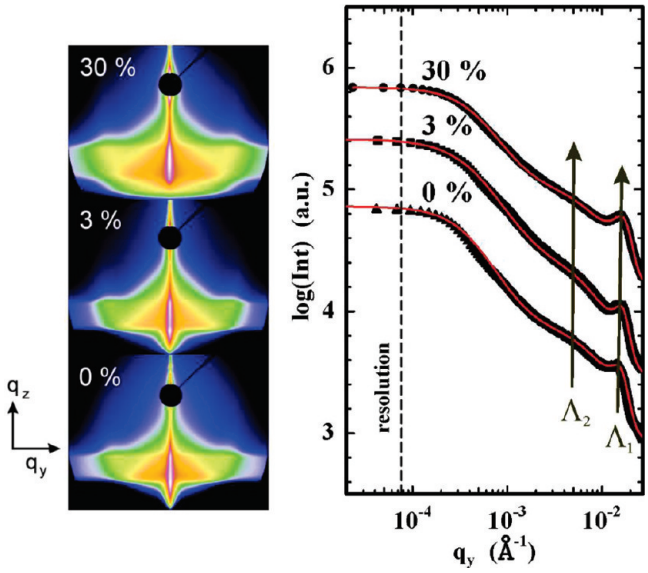

FIGURE 7. GISAXS scattering images (left) and corresponding cuts (right) of titania films with different degrees of microstructuring. Solid lines are fits to the data. The cuts show two peaks corresponding to the two preferred lateral lengths Λ_1 and Λ_2 in the films.

970 g cm^{-3} and a porosity of 75%. For the calcined film, in accordance with the larger film thickness and the larger pore size, a low density of 600 g cm^{-3}, corresponding to 84% porosity, is found. These values show the high porosity of the films and also the extension of the pore structure into the bulk of the films. From the high porosity a high surface area of the films can be concluded, which is one prerequisite for the creation of a large interface with hole conducting material.

GISAXS was also used to quantify the influence of the PMMA on the pore structure. The 2D scattering images together with the cuts are shown in Figure 7. From the images as well as the cuts it is visible that addition of PMMA particles to the sol–gel solution modifies the film morphology. All cuts show a marked shoulder corresponding to a preferred structural length of the mesopores and, at higher q_y values, a broad shoulder originating from the macropores. Whereas the lateral dimension of the macropores remains constant within experimental error, the size of the mesopores decreases from 40 to 37 nm with a PMMA particle addition of 30% to the sol–gel solution (Figure 8). Because the GISAXS signal is averaged over a macroscopic sample area, these values do not just reflect local inhomogeneities but are characteristic for the whole film and thus represent differences induced by the preparation method. Due to the chemical similarity of PMMA and MA(PEO), the etching of the PMMA microspheres by the THF in the sol–gel solution is equal to the addition of a homopolymer to a micellar solution of a diblock copolymer, where one block is similar to the added homopolymer. In such systems the homopolymer is expected to accumulate in this block and to swell the micelles. When the film is prepared from the solution with the swollen micelles, the size and morphology of the resulting titania structures are modified: i.e., the titania network is extended and the size of the incorporated mesopores is

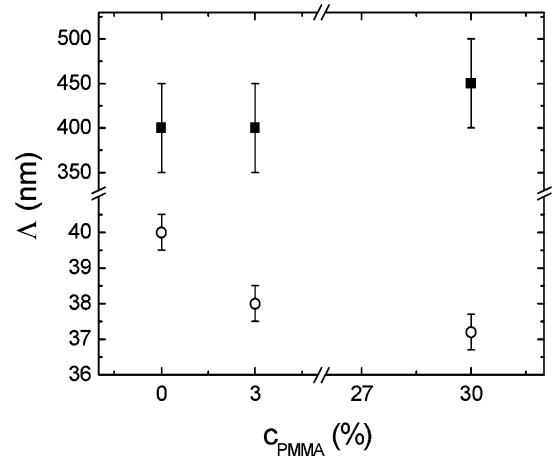

FIGURE 8. Preferred lateral lengths Λ_1 (open circles) and Λ_2 (solid squares) with changing PMMA particle addition. The size of the mesopores decreases with increasing amounts of PMMA particles added to the sol–gel solution.

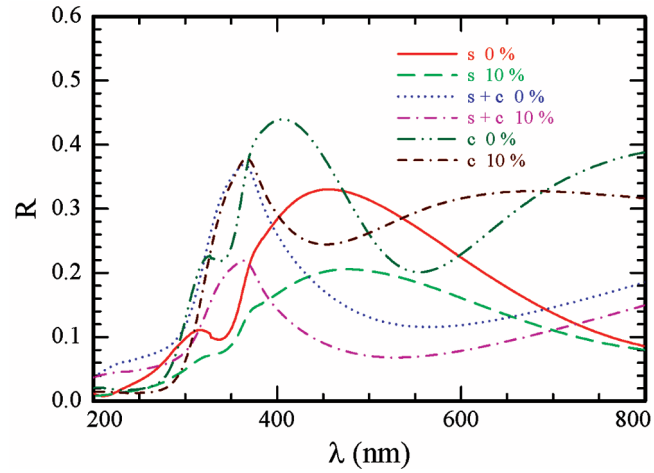

FIGURE 9. Reflectivity of films without microstructure (0% PMMA) and a surface structure created by addition of 10% PMMA microspheres. Acetic acid treated films (s, s + c) show a higher reduction in reflectivity than the directly calcined (c) film.

reduced. This micellar swelling provides a simple way for fine-tuning of the desired film structure (42).

To quantify the effect of the microstructure on the light absorption behavior, the reflectivity of the films microstructured by 10% PMMA particle addition was measured with UV/vis spectroscopy and compared with the reflectivity of films without microstructure (Figure 9). At low wavelengths the reflected intensity is low, because of the absorption bands of the titania. Above 400 nm, where titania becomes transparent, absorption is negligible and the interaction with the film structure determines the reflectivity spectra. Because the size of the mesopores is far below the wavelength of visible light, the mesopore structure does not contribute to the scattering and the film reflectivity is only modified by the large-scale structures. Independent of the method of polymer extraction the reflectivity of the microstructured films is considerably decreased in comparison to that of an unstructured film. With calcination directly applied to the nanocomposite film, the maximum reflectivity of the microstructured film is about 15% lower than the maximum reflectivity of the unstructured film; additionally, the reflec-

tivity spectrum is shifted toward smaller wavelengths, which results in an effective reduction in reflectivity in the spectral range between 360 and 500 nm up to 35% and an increase of the same order between 500 and 690 nm. By application of polymer extraction with acetic acid the reflectivity in the uncalcined film is strongly reduced over the whole spectral range. The maximum reduction is obtained in the range of visible light, which is of particular interest due to the absorption characteristics of many application-relevant polymers. By subsequent calcination a further reduction in reflectivity to absolute values below 0.1 is achieved. The remarkable difference from the directly calcined films is a result of the modification of the surface structure by the acetic acid. The erosion of the structural features acts as an effective roughening of the surface (see also Figure 1 for comparison) on the size scale of the macropores, which enhances light scattering and thus decreases the film reflectivity. Consequently, from the point of application, polymer extraction with acetic acid followed by calcination is the method of choice to obtain films with low surface reflection and enhanced scattering to trap a higher portion of light.

CONCLUSIONS

In summary, we show a simple one-step route for preparation of hierarchically structured titania films with functionality for application in photovoltaics provided by three structural levels. A sol−gel process with the diblock copolymer PDMS-*b*-MA(PEO) as structure directing agent is combined with the addition of PMMA microspheres to the sol−gel solution as a secondary template. The films show a mesoporous structure on the nanometer scale, with pores 35−40 nm in size opening the possibility for the infiltration of hole conducting materials with large dimensions. Additionally, the surface is roughened by macropores, which provide channels for an improved infiltration of the hole conducting material. Well-defined surface depressions of 1 μm in diameter are introduced as light scatterers for the reduction of surface reflection and enhancement of absorption. To our knowledge this is the first time that porous films with large mesopores for application in photovoltaics have been additionally structured on a micrometer scale to reduce light reflection.

The structure installed in the titania films depends on the method of extracting the polymer templates from the nanocomposite film; calcination results in larger meso- and macropores than extraction with acetic acid, and acetic acid treated films have a more eroded surface. Already a moderate degree of microstructuring by PMMA microspheres results in a significant reduction of reflectivity; a minimum reflectivity value favorable for application in a photovoltaic device is obtained by treatment with acetic acid and subsequent calcination. The addition of the PMMA microspheres to the sol−gel solution influences the film structure on all levels; with addition of a high amount of PMMA the films have a lower degree of order. Additionally the size of the mesopores is decreased. This shows that within the complex interplay of all components involved in the sol−gel process by addition of a second templating polymer not only a further structure is created but also already existing primary structural features are influenced. While the interaction with colloidal particles can completely disrupt the primary structure, it is also possible to use a more controlled block-copolymer/colloid interaction to adjust the morphology of the primary structure. The latter case then opens a simple way to fine-tune the block-copolymer templated structure to meet the requirements of a working device even more closely.

It remains a promising future work to further adjust the pore structure as well as to test the suitability of the presented route in other film preparation methods and, ultimately, to apply the structured films in photovoltaic devices.

Acknowledgment. We thank A. Timmann for the assistance in the GISAXS measurements. This work was financially supported by the Deutsche Forschungsgemeinschaft in the priority program SPP 1181 "Nanomat" (GU771/2 and MU1487/5). M.A.R. acknowledges the Bavarian State Ministry of Sciences, Research and Arts for funding this research work through the International Graduate School 'Materials Science of Complex Interfaces' (CompInt).

REFERENCES AND NOTES

(1) Kay, A.; Grätzel, M. *Sol. Energy Mater. Sol. Cells* **1999**, *44*, 99.
(2) Arango, A. C.; Johnson, L. R.; Bliznyuk, V. N.; Schlesinger, Z.; Carter, S. A.; Hörhold, H. H. *Adv. Mater.* **2000**, *12*, 1689.
(3) Fujishima, A.; Rao, T. N.; Tryk, D. A. *J. Photochem. Photobiol. C* **2000**, *1*, 1.
(4) Choi, H.; Sofranko, A. C.; Dionysiou, D. D. *Adv. Funct. Mater.* **2006**, *16*, 1067.
(5) Varghese, O. K.; Gong, D.; Paulose, M.; Ong, K. G.; Grimes, C. A. *Sens. Actuators B* **2003**, *93*, 338.
(6) Chuangchote, S.; Jitputti, J.; Sagawa, T.; Yoshikawa, S. *ACS Appl. Mater. Interfaces* **2009**, *1*, 1140.
(7) O'Reagan, B.; Grätzel, M. *Nature* **1991**, *353*, 737.
(8) O'Hayre, R.; Nanu, M.; Schoonman, J.; Goossens, A.; Wang, Q.; Grätzel, M. *Adv. Funct. Mater.* **2006**, *16*, 1566.
(9) Lancelle-Beltran, E.; Prené, P.; Boscher, C.; Belleville, P.; Buvat, P.; Sanchez, C. *Adv. Mater.* **2006**, *18*, 2579.
(10) Sanchez, C.; Boissière, C.; Grosso, D.; Laberty, C.; Nicole, L. *Chem. Mater.* **2008**, *20*, 682.
(11) Yelamanchili, R. S.; Lu, Y.; Lunkenbein, T.; Miyajima, N.; Yan, L.; Ballauff, M.; Breu, J. *Small* **2009**, *5*, 1326.
(12) Lee, J.; Orilall, M. C.; Warren, S. C.; Kampermann, M.; Disalvo, F. J.; Wiesner, U. *Nat. Mater.* **2008**, *7*, 222.
(13) Sakatani, Y.; Boissière, C.; Grosso, D.; Nicole, L.; Soler-Illia, G. J. A. A.; Sanchez, C. *Chem. Mater.* **2008**, *20*, 1049.
(14) Song, J. H.; Kretzschmar, I. *ACS Appl. Mater. Interfaces* **2009**, *1*, 1747.
(15) Yuan, Z. Y.; Su, B. L. *Colloids Surf. A* **2004**, *241*, 173.
(16) Cheng, Y.; Gutmann, J. S. *J. Am. Chem. Soc.* **2006**, *128*, 4658.
(17) Lan, Y.; Gao, X. P.; Zhu, H. Y.; Zheng, Z. F.; Yan, T. Y.; Wu, F.; Ringer, S. P.; Song, D. Y. *Adv. Funct. Mater.* **2005**, *15*, 1310.
(18) Kaper, H.; Endres, F.; Djerdi, I.; Antonietti, M.; Smarsly, B. M.; Maier, J.; Hu, Y. S. *Small* **2007**, *10*, 1753.
(19) Smarsly, B.; Grosso, D.; Brezesinski, T.; Pinna, N.; Boissière, C.; Antonietti, M.; Sanchez, C. *Chem. Mater.* **2004**, *16*, 2948.
(20) Kim, D. H.; Sun, Z.; Russell, T. P.; Knoll, W.; Gutmann, J. S. *Adv. Funct. Mater.* **2005**, *15*, 1160.
(21) Deshpande, A. S.; Shchukin, D. G.; Ustinovich, E.; Antonietti, M.; Caruso, R. A. *Adv. Funct. Mater.* **2005**, *15*, 239.
(22) Perlich, J.; Kaune, G.; Memesa, M.; Gutmann, J. S.; Müller-Buschbaum, P. *Philos. Trans. R. Soc. A* **2009**, *367*, 1783.
(23) Mahajan, S.; Renker, S.; Simon, P. F. W.; Gutmann, J. S.; Jain, A.; Gruner, S. M.; Fetters, L. J.; Coates, G. W.; Wiesner, U. *Macromol. Chem. Phys.* **2003**, *204*, 1047.
(24) Finnefrock, A.; Ulrich, R.; Du Chesne, A.; Honeker, C.; Schumacher, K.; Unger, K.; Gruner, S.; Wiesner, U. *Angew. Chem., Int. Ed.* **1999**, 1208.
(25) Yuan, Z.; Su, B. *J. Mater. Chem.* **2006**, *16*, 663.
(26) Yu, J. G.; Su, Y. R.; Cheng, B. *Adv. Funct. Mater.* **2007**, *17*, 1984.

(27) Huang, C.; McClenaghan, N. D.; Kuhn, A.; Bravic, G.; Bassani, D. M. *Tetrahedron* **2006**, *62*, 2050.
(28) Usami, A. *Chem. Phys. Lett.* **1997**, *277*, 105.
(29) Yang, P.; Deng, T.; Zhao, D.; Feng, P.; Pine, D.; Chmelka, B. F.; Whitesides, G. M.; Stucky, G. D. *Science* **1998**, *282*, 2244.
(30) Cecilia Fuertes, M.; Soler-Illia, G. J. A. A. *Chem. Mater.* **2006**, *18*, 2109.
(31) Malfatti, L.; Bellino, M. G.; Innocenzi, P.; Soler-Illia, G. J. A. A. *Chem. Mater.* **2009**, *21*, 2763.
(32) Zhao, Y.; Zhai, J.; Tan, S.; Wang, L.; Jiang, L.; Zhu, D. *Nanotechnology* **2006**, *17*, 2090.
(33) Memesa, M.; Weber, S.; Lenz, S.; Perlich, J.; Berger, R.; Müller-Buschbaum, P.; Gutmann, J. S. *Energy Environ. Sci.* **2009**, *2*, 783.
(34) Velev, O. D.; Lenhoff, A. M. *Curr. Opin. Colloid Interface Sci.* **2000**, *5*, 56.
(35) Klein, S. M.; Manoharan, V. N.; Pine, D. J.; Lange, F. F. *Colloid Polym. Sci.* **2003**, *282*, 7.
(36) Müller-Buschbaum, P. *Eur. Phys. J. E* **2003**, *12*, 443.
(37) Roth, S. V.; Döhrmann, R.; Dommach, M.; Kuhlmann, M.; Kröger, I.; Gehrke, R.; Walter, H.; Schroer, C.; Lengeler, B.; Müller-Buschbaum, P. *Rev. Sci. Instrum.* **2006**, *77*, 085106.
(38) Gutmann, J. S.; Müller-Buschbaum, P.; Stamm, M. *Faraday Discuss.* **1999**, *112*, 285.
(39) Soler-Illia, G. J. A. A.; Crepaldi, E. L.; Grosso, D.; Sanchez, C. *Curr. Opin. Colloid Interface Sci.* **2003**, *8*, 109.
(40) Müller-Buschbaum, P. *Anal. Bioanal. Chem.* **2003**, *376*, 3.
(41) Salditt, T.; Metzger, T. H.; Peisl, J.; Reinker, B.; Moske, M.; Samwer, K. *Europhys. Lett.* **1995**, *32*, 331.
(42) Perlich, J.; Schulz, L.; Abul Kashem, M. M.; Cheng, Y.; Memesa, M.; Gutmann, J. S.; Roth, S. V.; Müller-Buschbaum, P. *Langmuir* **2007**, *23*, 10299.

AM900592U